Journal of
Materials Chemistry A

Accepted Manuscript

This article can be cited before page numbers have been issued, to do this please use: J. Li, X. Zhou, Z. Xia, Z. zhang, J. Li, Y. Ma and Y. Qu, *J. Mater. Chem. A*, 2015, DOI: 10.1039/C5TA03153B.

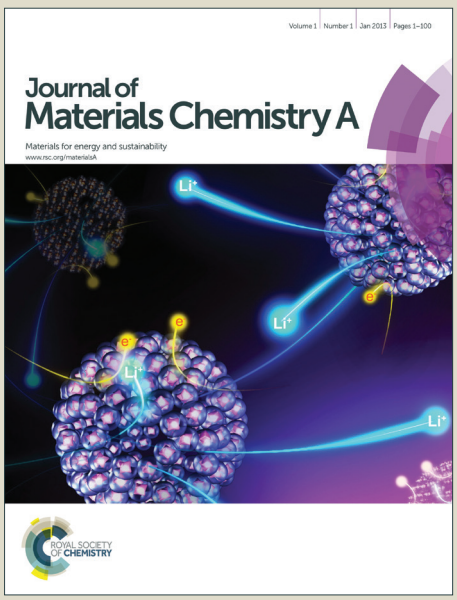

ROYAL SOCIETY OF CHEMISTRY

www.rsc.org/materialsA

View Article Online
DOI: 10.1039/C5TA03153B

Journal Name

RSCPublishing

ARTICLE

Facile synthesis of CoX (X=S, P) as efficient electrocatalysts for hydrogen evolution reaction

Cite this: DOI: 10.1039/x0xx00000x

*Jiayuan Li[a], Xuemei Zhou[a], Zhaoming Xia[a], Zhiyun Zhang[a], Jing Li[a], Yuanyuan Ma[*ab], Yongquan Qu[*abc]*

Received 00th January 2012,
Accepted 00th January 2012

DOI: 10.1039/x0xx00000x

www.rsc.org/

Developing the environment-friendly and earth-abundant electrocatalysts is desired for efficient hydrogen evolution reaction (HER). Here we report a facile and controllable synthesis of CoX (X=S, P) nanocatalysts by chemical conversion of thin $Co(OH)_2$ nanoplates at the mild conditions. Both catalysts delivered the high catalytic activity for HER. The small onset potentials of 59 and 32 mV, along with the low Tafel slopes of 56.2 and 54.8 mV/dec, were observed for CoS and CoP, respectively. Analyses suggest that the better HER performance of CoP nanocatalysts could be attributed to their intrinsically more positive charged nature of the metal center Co, longer Co−P bond length, and more catalytic active sites due to the smaller size of the CoP nanocatalysts. The high catalytic stability in acidic media was also observed for both CoS and CoP catalysts for a duration of 18 hours.

Introduction

The increasing shortage of fossil fuels and the raising deteriorated effect on the environmentals by extensive usage of fossil fuels have already become obstacles to the sustainable development of human society.[1] A feasible solution is to search for the sustainable, clean and high-efficient energy resources as the alternatives.[2] Hydrogen possesses a very high calorific value which makes it as the promising alternative fuel in the future.[3] The water electrolysis is an important pathway to obtain molecular hydrogen with high purity for future applications. Therefore, the efficient and robust catalysts with the low reaction overpotential are expected for the hydrogen evolution reaction (HER) in the water splitting process.[4] Platinum (Pt), as the most effective HER catalyst, is a rare metal and expensive which limits its widespread use.[5] The earth-abundant nickel-based alloys as the commercial HER catalyst with the high performance exhibit a low catalytic stability in the acidic electrolyte media.[6-9] Recently, MoS_2, as an acid-stable HER catalyst, has already been considered as a promising substitution for Pt owing to its relative abundant reserve and high HER intrinsic catalytic activity.[10-14] However, the bulk MoS_2 shows a poor HER performance.[15] The superior HER performance of MoS_2 depends on the artificially designed nanostructure with more edge activity sites.[16-20] Meanwhile, the low chemical stability of MoS_2 due to the oxidation in the presence of oxygen further limits its application.[16]

Hence, the great efforts have been focused on the earth-abundant transition metal (Co, Ni, Fe) sulfides/phosphides,[21-25] which can deliver high catalytic activity toward HER and good catalytic stability in acidic media. The previous works have reported that the cobalt-based sulfides/phosphides share the same catalytic mechanism as the hydrogenase happened in nature.[21, 23] On the basis of the catalytic mechanism, the metal center cobalt serves as the active sites.[18] Specifically, the function of cobalt is the hydride-acceptor center and the corresponding pendant base is the proton-acceptor.[24, 26] Cooperatively, hydrogen can be generated. However, there exists considerable differences in the HER performance of the cobalt-based sulfides and phosphides even though the corresponding pendant base S and P have the nearby atomic number in periodic table of elements.[23, 27] CoP nanowires[23] exhibited HER performance with an onset potential of 38 mV, a Tafel slope of 51 mV/dec, and an overpotential of 100 mV to reach the current density of 20 mA/cm^2. Meanwhile, CoS_2 nanowires[27] delivered an onset potential of 75 mV and a Tafel slope of 51.6 mV/dec for HER. To achieve the current density of 20 mA/cm^2, the overpotential of 160 mV was required. The

View Article Online
DOI: 10.1039/C5TA03153B
Journal Name

performance of CoS_2 film[27] was also studied, in which the onset potential of 119 mV, the Tafel slope of 51.4 mV/dec and the overpotential of 206 mV for the catalytic current density of 20 mA/cm^2 were observed. Obviously, the atomic configurations and morphology characteristics of cobalt-based sulfides and phosphides play important roles in their HER performance. However, the specific contribution of the atomic configurations and morphology characteristics to their HER performance is still unclear owing mainly to the lack of relevant experimental investigations.

In this work, we reported a facile and controllable synthetic approach by chemically converting the thin $Co(OH)_2$ nanoplate precursor into CoX (X=S, P) nanostructures. The powder X-ray diffraction (XRD), X-ray photoelectron spectroscopy (XPS) and transmission electron microscope (TEM) were used for identifying the phase changes and morphology features of CoX (X=S, P) while the electrochemical analyzer was utilized to evaluate their HER performance. The electrochemical measurements reveal the superior HER performance of both CoS and CoP nanocatalysts with the small onset overpotential of 59 and 32 mV and the low Tafel slopes of 56.2 and 54.8 mV/dec, respectively. The experimental results suggest that the superior HER performance of CoP could be derived from its intrinsically positive charged nature of the metal center Co, the long bond length of Co−P and the abundant catalytic active sites toward HER.

Experimental

All chemicals used in the experiments are analytical grade and used as received without further purification.

Synthesis of thin β-$Co(OH)_2$ nanoplates

β-$Co(OH)_2$ nanoplates were synthesized through the same process as demonstrated in our previous work[28]. Specifically, NaOH (0.16 mol) was dissolved in 35 mL of Milli-Q water. $Co(NO_3)_2$. $6H_2O$ aqueous solution (4.0 M) was slowly injected into the NaOH aqueous solution. After stirring continuously for 30 min, the mixture was transferred into an electric oven at 100 °C for 12 hours. The β-$Co(OH)_2$ nanoplates was centrifugated off, thoroughly washed with copious amount of deionized water and ethanol for several times, and then dried in vacuum at 60 ºC overnight.

Synthesis of CoS nanocatalysts

Anion exchange reaction was utilized for synthesis of CoS nanocatalysts. Briefly, as-prepared $Co(OH)_2$ precursor (50 mg) was well suspended in 12.5 mL of deionized water through ultrasonication at room temperature. Sodium sulfide (0.5 g) was slowly added into the brown β-$Co(OH)_2$ nanoplate colloidal solution sequentially. The solution was stirred at room temperature for 10 min and then transferred into a 20 mL Teflon-lined autoclave. The reaction was maintained at 80 ºC for 12 h. The CoS nanocatalysts was obtained after centrifugation and thorough washing with deionized water for three times and then dried in vacuum at 60 ºC for 12 h.

Synthesis of CoP nanocatalysts

CoP nanocatalysts were synthesized through a solid-phase reaction between β-$Co(OH)_2$ nanoplates and NaH_2PO_2. For a typical synthesis, 27.9 mg of β-$Co(OH)_2$ nanoplate precursor and 159 mg of NaH_2PO_2 were mixed together and ground into a fine powder by using a mortar. Then, the mixture was calcined at 300 ºC for 2h in a quartz tube with a ramping rate of 2 ºC/min under a flow of argon. The obtained product was thoroughly washed with deionized water for the removal of the surplus salts. The CoP nanocatalysts were dried in vacuum at 60 ºC for 12 h.

Characterization

The phase evolution of as-synthesized nanostructures was monitored by powder XRD. The XRD patterns with diffraction intensity versus 2θ were recorded in a Shimadzu X-ray diffractometer (Model 6000) using Cu Kα radiation. XPS spectra were acquired on a Thermo Electron Model K-Alpha with Al Kα as the excitation source. TEM images and high-resolution TEM (HRTEM) images were taken with a Tecnai G2 F20 S-twin transmission electron microscope with an accelerating voltage of 120 kV. The surface area was evaluated by nitrogen physisorption (Micromeritics, ASAP 2020 HD88) based on the Brunauer-Emmet-Teller (BET) method.

Electrochemical measurements

Electrochemical measurements were performed with a CHI 660D electrochemical analyzer (CH Instruments, Inc., Shanghai). All the electrochemical measurements were conducted by a typical three-electrode setup with an electrolyte solution of 0.5 M H_2SO_4, a Pt counter electrode, and a saturated calomel electrode (SCE) reference electrode. The preparation method of the working electrodes containing HER catalysts was described as follows. Briefly, the catalyst ink was prepared by dispersing 4 mg of catalyst into 1 mL of water/ethanol (v/v=768: 200) solvent containing 32 μL of 5 wt% Nafion. Then 5 μL of this catalyst ink (containing 20 μg of catalyst) was loaded onto a carbon fiber paper to achieve the sample loading ~0.91 mg/cm^2. The SCE reference electrode was calibrated with respect to reversible hydrogen electrode (RHE) by adding a value of (0.242 +0.059pH) V before the measurements. Linear Sweep Voltammetry (LSV) measurements were performed with a scan rate of 5 mV/s. The onset potentials were determined based on the beginning of linear regime of the Tafel plot. The time dependency of catalytic currents during electrolysis for the catalyst was tested in 0.5 M H_2SO_4 at η=121 mV after equilibrium. Electrochemical impedance spectroscopy (EIS) measurements were carried out on the AUTOLAB PGSTAT204 electrochemistry workstation in the frequency range from 100 kHz to 0.1 Hz at an open circuit potential, with 10 mV as the amplitude potential.

Journal Name

View Article Online
DOI: 10.1039/C5TA03153B

Results and discussion

β-$Co(OH)_2$ nanoplates were synthesized by the co-precipitation method at 100 ºC for 12h.[28] The phase and microstructures of the as-synthesized nanostructures were characterized by powder XRD and electron microscopy, respectively. XRD pattern (Fig. 1a, black curve) indicates the as prepared nanostructures are β-$Co(OH)_2$ phase (JCPDS-45-0031).[28] Similar to our previous report, the nanostructures exhibit a plate-like morphology (Fig. 1b).[28] A wide distribution from tens of nanometers to hundreds of nanometers was observed.

β-$Co(OH)_2$ nanoplates were employed as the precursors and converted into cobalt sulfides and phosphides through the anion exchange method and the high temperature reaction approach, respectively. It was found that the β-$Co(OH)_2$ nanoplates were completely converted into sulfides or phosphides, based on their XRD patterns (Fig. 1a). The XRD patterns of as-obtained nanostructures can be well indexed to the hexagonal CoS phase (JCPDS-75-0605, blue curve)[29] and the orthorhombic CoP phase (JCPDS-29-0497, red curve).[22] TEM images (Fig. 1c and 1d) reveal that the plate-like morphology of the CoS products was well preserved after the sulfidation reaction. The interconnected or merged plates were also observed. The slight transparent of the CoS plates under the electron beam indicates the thin nature of as-prepared nanostructures. The calculated lattice fringe of 0.291 nm from HRTEM (Fig. 1d) was corresponded to the (100) crystal surface of the hexagonal CoS phase, further indicating the formation of CoS nanoplates. After phosphidation, a structural deformation for as-prepared CoP was observed (Fig. 1e), in which the crystalline size of CoP exhibits a dramatically decrease from tens of nanometers of the β-$Co(OH)_2$ nanoplate precursor to several nanometers. TEM image (Fig. 1e) also reveals that the small crystalline of CoP was integrated into a large porous structure. This morphological transformation can be attributed to the effect of PH_3 generated by the decomposition of NaH_2PO_2 in the solid-phase reaction and the structural collapse of the thin nanoplate precursor at high temperatures.[30, 31] The measured lattice spacing was 0.279 nm (HRTEM image, Fig. 1f), which corresponded to the (002) plane of the orthorhombic CoP phase.

XPS technique was employed to investigate the electronic structures of the as-prepared CoS and CoP nanocatalysts. All the spectra were referenced to the aliphatic carbon at a binding energy (BE) of 284.5 eV. The XPS survey spectra of the as-prepared samples were shown in the Supporting Information Fig. S1, which reveals the final products are CoS and CoP. Fig. 2a and 2b present the high resolution XPS spectra of CoP at Co 2p and P 2p regions. Two apparent peaks at 779.2 and 781.7 eV in the energy level of Co 2p3/2 (Fig. 2a) can be assigned to the positive charged Co in CoP[32] and the oxidized Co species.[33] As shown in XPS spectrum of P (Fig. 2b), three peaks at 129.7, 130.8 and 134.0 eV are observed. The peaks at 129.7 eV and 130.8 eV can be assigned to P 2p3/2 and P 2p1/2 in CoP.[32] The weak peak at 134.0 eV can be attributed to the oxidized P species[33]. The presence of the oxidized Co and P species can be

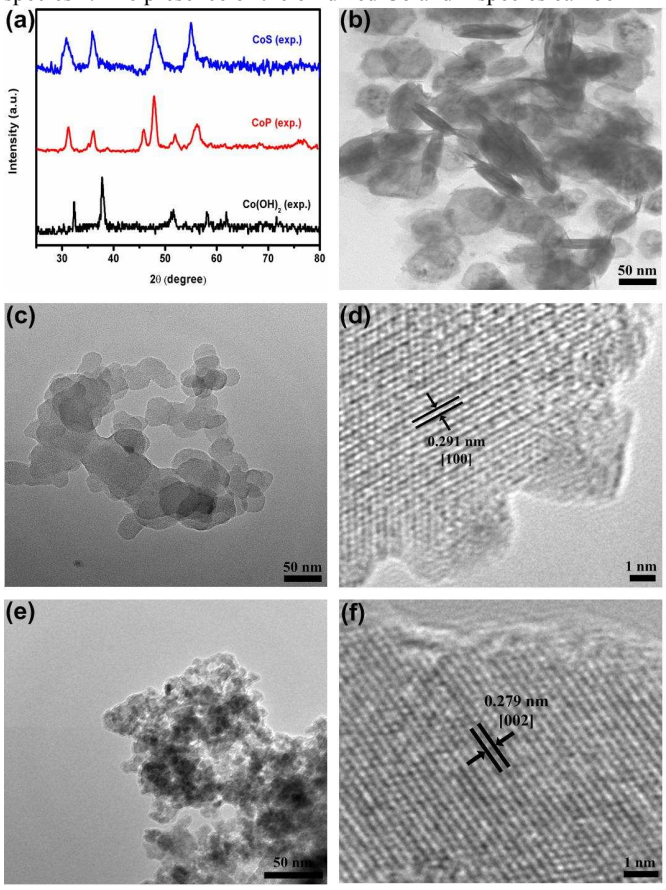

Fig. 1 Structural characterizations of β-$Co(OH)_2$ nanoplate, CoS and CoP catalysts. (a) Powder XRD patterns of β-$Co(OH)_2$ nanoplate precursor and as-prepared CoP and CoS. (b) TEM image of β-$Co(OH)_2$ nanoplates. (c) TEM image of CoS. (d) HRTEM image of CoS. (e) TEM image of CoP. (f) HRTEM image of CoP.

attributed to the superficial oxidation of CoP sample in air, similar to previous studies.[33] Similarly, the peaks at 779.0 and 162.2 in the Co 2p3/2 and S 2p3/2 region corresponded to the binding energy of Co and S in CoS.[34] Meanwhile, the peaks at 781.4 eV of Co 2p3/2 and 168.0 eV of S 2p3/2 manifest the superficial oxidation in CoS nanocatalysts upon the exposure to air.[34] Compared with the binding energy of Co metal (778.1–778.2 eV) and elemental S or P (130.2 or 163.7 eV),[35] the energy level of Co 2p3/2 in both CoS and CoP shifts to high energy, indicating the Co atom in both CoS and CoP with a partial positive charge (δ^+). In contrast, the energy levels of S 2p3/2 and P 2p3/2 in CoS and CoP exhibit a negative shift compared to those of elemental S and P, suggesting the partially negative charged S and P (δ^-). The XPS spectra manifest a charge transfer process from metal Co to P or S,[32, 36] which is desired for high performance HER electrocatalysis.

To evaluate the HER activities of the CoS and CoP, the catalysts were loaded onto and carbon fiber paper (CFP) substrates with a density of 0.91 mg cm^{-2} by drop casting. The LSV curves of the bare CFP substrate, CoS and CoP electrodes in 0.5 M H_2SO_4 electrolyte at a scan rate of 5 mV/s are shown in Fig. 3a. Compared to the strong catalytic current densities of

View Article Online
DOI: 10.1039/C5TA03153B
Journal Name

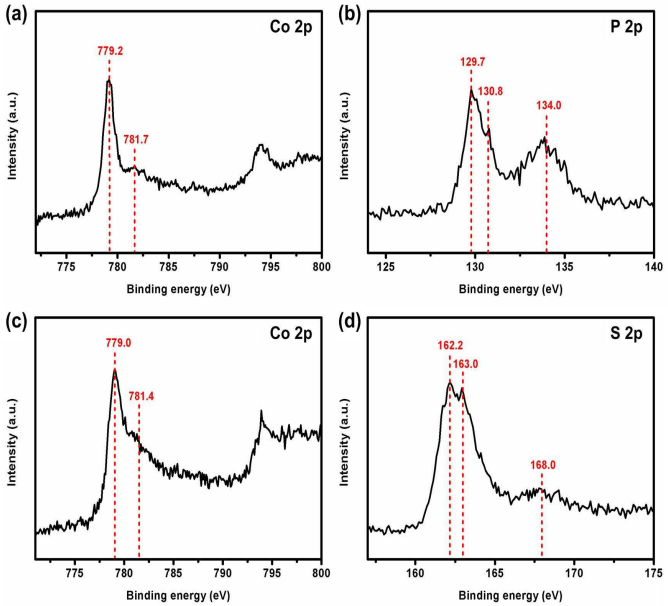

Fig. 2 The XPS fine spectra of (a) Co 2p and (b) P 2p region for CoP sample. The XPS fine spectra of (c) Co 2p and (d) S 2p region for CoS sample.

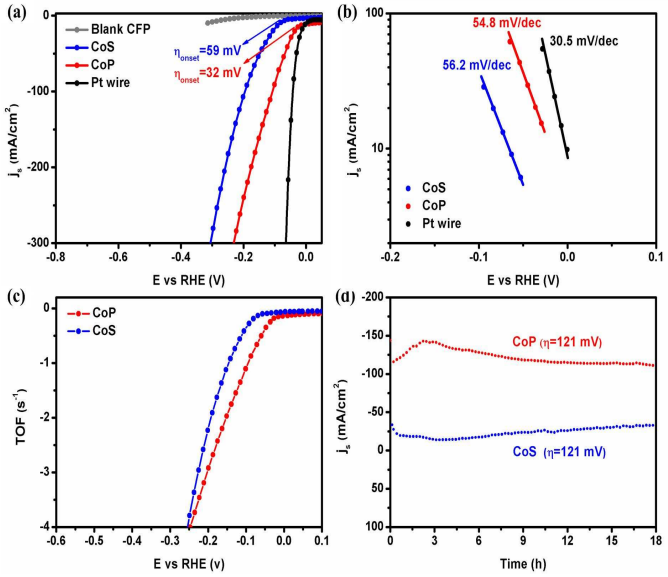

Fig. 3 HER catalytic activity of the CoS and CoP nanocatalysts. (a) Polarization curves for Pt wire, CoS, CoP and blank carbon fiber paper (CFP) at a scan rate of 5 mV/s. (b) The corresponding Tafel plots for Pt wire, CoS and CoP. (c) The calculated turnover frequency curves for CoS and CoP nanocatalysts in our experiment. (d) Time-dependent current density.

the CoS and CoP catalysts, the very weak current density (2.9 mA cm^{-2}) of the CFP substrate at 0.2 V applied potential (vs RHE) indicates the inactive nature of CFP towards HER and a background correction for the CFP substrate is unnecessary for all catalytic electrodes.

As a comparison, the catalytic activity of the commercially available Pt wire was also evaluated as shown in Fig. 3a. Pt wire exhibits the expected catalytic activity with the near zero onset overpotential and high HER catalytic activity at each bias. Notably, both as-synthesized CoS and CoP deliver good HER catalytic activity as reflected by their small onset potentials and large HER current densities at the specific applied voltages. The CoP catalysts exhibited a higher HER catalytic activity than the CoS catalysts under the identical conditions. The onset potential of 32 mV for CoP catalysts was 27 mV smaller than that (59 mV) for CoS in the acidic media (0.5 M H_2SO_4). An overpotential of 107 mV of the CoP electordes realized a catalytic HER current densities of 100 mA/cm^2. In contrast, a high overpotential of 196 mV for CoS was required to achieve the catalytic current densities of 100 mA/cm^2.

We also fitted the polarization curves of the Pt wire, CoP and CoS shown in Fig. 3a to the Tafel equation. As presented in Fig. 3b, the derived Tafel slope for the Pt wire is 30.5 mV/dec, consistent with the previously reported values.[22] The values of Tafel slope for CoS and CoP nanocatalysts (Fig. 3b) are 56.2 and 54.8 mV/dec in the region of 5-60 mV, respectively. Those values are comparable to or even better than those of cobalt-based sulfides/phosphides[23, 27, 31, 37] and those of many acid-stable Mo, Fe and Ni based HER catalysts previously reported.[16, 24, 25, 38, 39] The values of Tafel slope also suggest the Volmer-Heyrovsky reaction mechanism for CoS and CoP as the HER catalysts.[40, 41] Also, the exchange current density (j_0) of CoS and CoP are calculated to be about 1.62×10^{-5} and 2.4×10^{-4} A/cm^2, which are close to the best reported results of the cobalt phosphides/sulfides[23, 27] and larger than most of the reported HER catalysts.[39] The exchange current density of CoP is estimated to be 15 times larger than CoS. The larger j_0 of CoP can be attributed to its morphology characteristics that possess the larger surface area and could provide more effective active sites.[42] More details will be discussed in the following.

The catalytic activity of each catalyst in terms of the values of turnover frequency (TOF) at each active site can be derived from the LSV curves shown in Fig. 3a. The number of the active sites was estimated by scanning the cyclic voltammetrys of the CoS and CoP electrodes in 1.0 M PBS (pH=7) with a potential window from −0.2 to 0.6 V vs RHE and a scan rate of 50 mV/s (Fig. S2).[43] The integrated charge within the scanning potential window is roughly proportional to the total number of the active sites of the electroactive materials. By assuming a one-electron process for both reduction and oxidation, the upper limit of the active site can be calculated. Details can be found in the Supplementary Information. Fig. 3c shows the calculated TOF curves of CoS and CoP in 0.5 M H_2SO_4 within the range of applied potentials. On the basis of previous works, Pt exhibits the best HER catalytic activity, which reaches a TOF of 0.8 s^{-1} at 0 V.[18] Compared with Pt, the overpotentials of 133 and 82 mV were required to achieve the TOF of 0.8 s^{-1} for CoS and CoP, respectively. In contrast, an overpotentials of 300 mV was needed for MoS_2 catalysts to realize a TOF of 0.725 s^{-1}, further indicating the high catalytic activity of the CoS and CoP catalysts.[44] To reach a TOF of 4 s^{-1}, the overpotentials of CoS and CoP are 253 and 246 mV, respectively, which are smaller than those of MoS_2-based nanowire catalyst (272 mV)[45] and close to the best reported results of the cobalt phosphides/sulfides (240 mV).[23]

Journal Name

View Article Online
DOI: 10.1039/C5TA03153B

Besides the catalytic stability, the catalytic stability of the CoS and CoP nanocatalytic was evaluated by running chronoamperometric response (i-t) at an overpotential of 121 mV in the acidic environments (0.5 M H_2SO_4). During the measurements, the working electrodes were continuously stirred at 1600 rpm to remove the generated hydrogen bubbles. The corresponding time-dependent current density curves are shown in Fig. 3d. Despite the fluctuation in the catalytic current density at the initial several hours, the stabilized catalytic current densities of CoS and CoP for HER were observed over 18 hours, indicating the high catalytic stability of both electroactive materials in the strong acidic aqueous solution.

Generally, it was found that the calculated TOFs of CoP were generally larger than those of CoS at the specific overpotentials (Fig. 3c), indicating the higher intrinsic catalytic activity of CoP over CoS. On the other hand, the TOF value of CoP is larger than CoS under the same overpotential, which can reveal the better intrinsic catalytic activity of CoP than CoS.[18] To understanding the native difference in the catalytic activity of CoS and CoP, the catalytic mechanism was studied. The superior HER performance of CoS and CoP nanocatalysts can derive from their similar catalytic domain to the hydrogenases, in which the active sites are characterized by the corresponding pendant bases proximate to the metal centers.[46] As shown in XPS spectra (Fig. 2), the surfaces of CoS or CoP is also characterized by the positively charged metal center Co (δ^+) with pendant base S or P (δ^-). Thus, it is expected that CoS and CoP share the similar HER catalytic mechanism to the hydrogenases.[23] On the basis of the hydrogenases catalytic mechanism, the metal center Co (δ^+) is the hydride-acceptor center and the pendant base S or P (δ^-) is proton-acceptor center, which can promote the HER and bring the high catalytic activity.[24, 26] The intrinsic catalytic activity of hydrogenases-like catalysts is highly relevant to the intrinsically charged nature of the metal center (δ^+)—a proportionality relationship between δ^+ value and the catalytic activity.[47-49] As revealed from XPS spectra (Fig. 2), more positive shift of Co 2p3/2 for CoP over CoS suggests the higher δ^+ of Co metal active sites for CoP, which can be use to explain the better intrinsic catalytic activity of the CoP catalysts.

In addition, the bond length between the metal center and its pendant base can also function as an indicator to the intrinsic catalytic activity.[50] The increase of the bond length between the metal active site and the corresponded pendant base favors the better electron localization on the corresponding pendant base and reduces the barrier to proton binding as a consequence.[50] The bond length of Co−P in CoP (2.3~2.4 Å)[51] is longer than that of Co−S in CoS (2.1~2.2 Å),[52] suggesting the high catalytic activity of CoP.

Meanwhile, CoP is a good conductor for charges,[32, 53] favoring the electron transfer of the CoP electrodes. As shown in electron impedance spectroscopy (Fig. 4), the Nyquist plots for both CoS and CoP electrodes show a semicircle, an indication of the conductivity of the electrodes. The calculated resistance of the CoP electrode (8.37 Ω) is much smaller than that of the CoS electrode (28.78 Ω), indicating a better electron

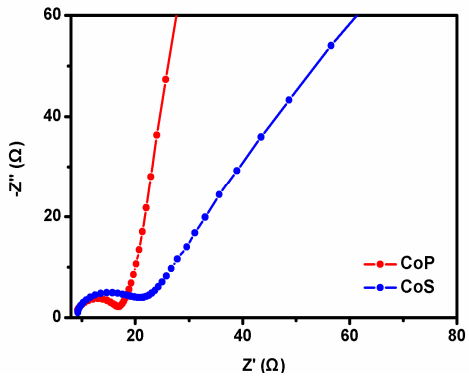

Fig. 4 Nyquist plots for CoS and CoP nanocatalysts.

transfer within the CoP electrode associated with a high HER catalytic activity.[49]

Given that the CoS and CoP share the same catalytic mechanism as hydrogenases, their morphological features also play an important role in their HER performance. For CoS, the plate-like morphology is preserved and interconnection between the plates is also observed. In contrast, the small crystalline of CoP is presented, which can be attributed to the evolution of PH_3 and high temperature annealing.[30, 31] The small crystalline size can provide more active sites. As evidenced from the N_2 adsorption-desorption isotherms, the BET surface area of CoP is 83.1 m^2/g, which is larger than that of CoS (28.1 m^2/g). Besides, more edges are exposed, which are generally considered as the catalytic sites with higher activity due to their low coordination numbers for HER. Therefore, with the same sample loading, the CoP with a small crystalline size associated with more surface active sites and more additional edge catalytic sites can qualitatively provide more catalytic active sites for HER. Conclusively, the higher catalytic activity of CoP can be rationalized as follows: (1) more positively charged metal of CoP; (2) Longer bond length of Co-P for improved electron delocalization during HER; (3) Higher electron conductivity of CoP and subsequent better charge transfer within the CoP electrode; and (4) More surface active sites and edge catalytic sites with high HER activity for CoP due to their morphological features.

Conclusions

In summary, CoX (X=S, P) nanocatalysts for HER was synthesized through via an anion exchange reaction and a high temperature phosphorizationm, in which thin β-$Co(OH)_2$ nanoplates were used as the precursor. The superior catalytic acitivity of both CoS and CoP were revealed by their small onset potential of 59 and 32 mV and the low Tafel slope of 56.2 and 54.8 mV/dec for CoS and CoP, respectively. The good catalytic stability was demonstrated by their stable HER catalytic current densities for a duration of 18 hours in acidic media. The results suggest the high catalytic activity of CoP over CoS, which can be attributed to the intrinsically charged nature of the metal center Co and the Co-X bond length, which corresponds to the positive relationship between the intrinsic

View Article Online
DOI: 10.1039/C5TA03153B
Journal Name

catalytic activity and the intrinsically positive charged nature of metal sites in CoP, the long bond length of Co-P, the high electron conductivity of CoP and more surface active sites and edge catalytic sites with high catalytic activity for CoP.

Acknowledgements

We acknowledge the financial support from a NSFC Grant 21201138 and 21401148. This work was also partially funded by the Ministry of Science and Technology of China through a 973-program under Grant 2012CB619401 and supported by the Fundamental Research Funds for the Central Universities under Grant xjj2013102 and xjj2013043. Technical supports for TEM experiments from Frontier Institute of Science and Technology and State Key Laboratory for Manufacturing Systems Engineering, Xi'an Jiaotong University, are also acknowledged.

Notes and references

[a] *Center of Applied Chemical Research, Frontier Institute of Science and Technology, Xi'an Jiaotong University, Xi'an, China 710049. E-mail: yongquan@mail.xjtu.edu.cn; yyma@mail.xjtu.edu.cn*

[b] *State Key Laboratory for Mechanical Behavior of Materials, Xi'an Jiaotong University, Xi'an, China, 710049.*

[c] *MOE Key Laboratory for Nonequilibrium Synthesis and Modulation of Condensed Matter, Xi'an Jiaotong University, Xi'an, China 710049*

† Footnotes should appear here. These might include comments relevant to but not central to the matter under discussion, limited experimental and spectral data, and crystallographic data.

Electronic Supplementary Information (ESI) available: TOF calculations and CV data. See DOI: 10.1039/b000000x/

1. Y. Qu and X. Duan, *Chem. Soc. Rev*. 2013, **42**, 2568-2580.
2. A. J. Bard and M. A. Fox, *Accounts Chem. Res.*, 1995, 28, 141-145.
3. M. Dresselhaus and I. Thomas, *Nature*, 2001, 414, 332-337.
4. J. A. Turner, *Science*, 2004, 305, 972-974.
5. M. G. Walter, E. L. Warren, J. R. McKone, S. W. Boettcher, Q. Mi, E. A. Santori and N. S. Lewis, *Chem. Rev.*, 2010, 110, 6446-6473.
6. J. R. McKone, B. F. Sadtler, C. A. Werlang, N. S. Lewis and H. B. Gray, *ACS Catal.*, 2013, 3, 166-169.
7. I. A. Raj and K. Vasu, *J. Appl. Electrochem.*, 1990, 20, 32-38.
8. A. Le Goff, V. Artero, B. Jousselme, P. D. Tran, N. Guillet, R. Métayé, A. Fihri, S. Palacin and M. Fontecave, *Science*, 2009, 326, 1384-1387.
9. M. Hambourger, M. Gervaldo, D. Svedruzic, P. W. King, D. Gust, M. Ghirardi, A. L. Moore and T. A. Moore, *J. Am. Chem. Soc.*, 2008, 130, 2015-2022.
10. A. B. Laursen, S. Kegnæs, S. Dahl and I. Chorkendorff, *Energ. Environ. Sci.*, 2012, 5, 5577-5591.
11. D. Merki and X. Hu, *Energ. Environ. Sci.*, 2011, 4, 3878-3888.
12. H. Vrubel, D. Merki and X. Hu, *Energ. Environ. Sci.*, 2012, 5, 6136-6144.
13. T. Wang, L. Liu, Z. Zhu, P. Papakonstantinou, J. Hu, H. Liu and M. Li, *Energ. Environ. Sci.*, 2013, 6, 625-633.
14. Y. Li, H. Wang, L. Xie, Y. Liang, G. Hong and H. Dai, *J. Am. Chem. Soc.*, 2011, 133, 7296-7299.
15. W. Jaegermann and H. Tributsch, *Prog. Surf. Sci.*, 1988, 29, 1-167.
16. J. Kibsgaard, Z. Chen, B. N. Reinecke and T. F. Jaramillo, *Nat. Mater.*, 2012, 11, 963-969.
17. D. Kong, H. Wang, J. J. Cha, M. Pasta, K. J. Koski, J. Yao and Y. Cui, *Nano lett.*, 2013, 13, 1341-1347.
18. T. F. Jaramillo, K. P. Jørgensen, J. Bonde, J. H. Nielsen, S. Horch and I. Chorkendorff, *Science*, 2007, 317, 100-102.
19. B. Hinnemann, P. G. Moses, J. Bonde, K. P. Jørgensen, J. H. Nielsen, S. Horch, I. Chorkendorff and J. K. Nørskov, *J. Am. Chem. Soc.*, 2005, 127, 5308-5309.
20. H. I. Karunadasa, E. Montalvo, Y. Sun, M. Majda, J. R. Long and C. J. Chang, *Science*, 2012, 335, 698-702.
21. D. Kong, J. J. Cha, H. Wang, H. R. Lee and Y. Cui, *Energ. Environ. Sci.*, 2013, 6, 3553-3558.
22. E. J. Popczun, C. G. Read, C. W. Roske, N. S. Lewis and R. E. Schaak, *Angew. Chem.*, 2014, 126, 5531-5534.
23. J. Tian, Q. Liu, A. M. Asiri and X. Sun, *J. Am. Chem. Soc.*, 2014, 136, 7587-7590.
24. E. J. Popczun, J. R. McKone, C. G. Read, A. J. Biacchi, A. M. Wiltrout, N. S. Lewis and R. E. Schaak, *J. Am. Chem. Soc.*, 2013, 135, 9267-9270.
25. Y. Xu, R. Wu, J. Zhang, Y. Shi and B. Zhang, *Chem. Communi.*, 2013, 49, 6656-6658.
26. P. Liu and J. A. Rodriguez, *J. Am. Chem. Soc.*, 2005, 127, 14871-14878.
27. M. S. Faber, R. Dziedzic, M. A. Lukowski, N. S. Kaiser, Q. Ding and S. Jin, *J. Am. Chem. Soc.*, 2014, 136, 10053-10061.
28. X. Zhou, Z. Xia, Z. Tian, Y. Ma and Y. Qu, *J. Mater. Chem. A*, 2015, 3, 8107-8114.
29. X. Xia, C. Zhu, J. Luo, Z. Zeng, C. Guan, C. F. Ng, H. Zhang and H. J. Fan, *Small*, 2014, 10, 766-773.
30. L. Song and S. Zhang, *Powder Technol.*, 2011, 208, 713-716.
31. Q. Liu, J. Tian, W. Cui, P. Jiang, N. Cheng, A. M. Asiri and X. Sun, *Angew. Chem.*, 2014, 126, 6828-6832.
32. A. P. Grosvenor, S. D. Wik, R. G. Cavell and A. Mar, *Inorg. Chem.*, 2005, 44, 8988-8998.
33. H. Li, P. Yang, D. Chu and H. Li, *Appl. Catal. A-Gen.*, 2007, 325, 34-40.
34. J.-Y. Lin and S.-W. Chou, *RSC Adv.*, 2013, 3, 2043-2048.
35. J. F. Moulder, J. Chastain and R. C. King, Handbook of X-ray photoelectron spectroscopy: a reference book of standard spectra for identification and interpretation of XPS data, Perkin-Elmer Eden Prairie, MN, 1992.
36. A. W. Burns, K. A. Layman, D. H. Bale and M. E. Bussell, *Appl. Catal. A-Gen.*, 2008, 343, 68-76.
37. Y. Sun, C. Liu, D. C. Grauer, J. Yano, J. R. Long, P. Yang and C. J. Chang, *J. Am. Chem. Soc.*, 2013, 135, 17699-17702.
38. Z. Xing, Q. Liu, A. M. Asiri and X. Sun, *Adv. Mater.*, 2014, 26, 5702-5707.
39. Z. Huang, Z. Chen, Z. Chen, C. Lv, M. G. Humphrey and C. Zhang, *Nano Energy*, 2014, 9, 373-382.
40. N. Pentland, J. M. Bockris and E. Sheldon, *J. Electrochem. Soc.*, 1957, 104, 182-194.
41. B. Conway and B. Tilak, *Electrochimica Acta*, 2002, 47, 3571-3594.
42. W. F. Chen, K. Sasaki, C. Ma, A. I. Frenkel, N. Marinkovic, J. T. Muckerman, Y. Zhu and R. R. Adzic, *Angew. Chem. Int. Edit.*, 2012, 51, 6131-6135.

Journal Name

View Article Online
DOI: 10.1039/C5TA03153B

43. D. Merki, S. Fierro, H. Vrubel and X. Hu, *Chem. Sci.*, 2011, 2, 1262-1267.

44. J. Xie, H. Zhang, S. Li, R. Wang, X. Sun, M. Zhou, J. Zhou, X. W. D. Lou and Y. Xie, *Adv. Mater.*, 2013, 25, 5807-5813.

45. Z. Chen, D. Cummins, B. N. Reinecke, E. Clark, M. K. Sunkara and T. F. Jaramillo, *Nano lett.*, 2011, 11, 4168-4175.

46. Y. Nicolet, A. L. de Lacey, X. Vernede, V. M. Fernandez, E. C. Hatchikian and J. C. Fontecilla-Camps, *J. Am. Chem. Soc.*, 2001, 123, 1596-1601.

47. A. R. Kucernak and V. N. N. Sundaram, *J. Mater. Chem. A*, 2014, 2, 17435-17445.

48. Y. Pan, Y. Liu, J. Zhao, K. Yang, J. Liang, D. Liu, W. Hu, D. Liu, Y. Liu and C. Liu, *J. Mater. Chem. A*, 2015, 3, 1656-1665.

49. T. Tian, L. Ai and J. Jiang, *RSC Adv.*, 2015, 5, 10290-10295.

50. G. C. Dismukes, A. B. Laursen, K. R. Patraju, M. Whitaker, M. Retuerto, T. Sarkar, N. Yao, K. V. Ramanujachary and M. Greenblatt, *Energ. Environ. Sci.*, 2015.

51. S. Rundqvist, *Acta. Chem. Scand.*, 1962, 16, 287-292.

52. P. Raybaud, J. Hafner, G. Kresse, S. Kasztelan and H. Toulhoat, *J. Catal.*, 2000, 190, 128-143.

53. Hulliger F. Crystal chemistry of the chalcogenides and pnictides of the transition elements, Springer Berlin Heidelberg, 1968, 83-229.